Spall fracture forms of high rock samples under uniaxial compression

Spall fracture forms of high rock samples under uniaxial compression

Leonid Vasyliev[1,5], Yurii Bulich[1], Dmytro Vasyliev[1], Mykola Malich[2], Zakhar Rizo[1], Alla Polishchuk[3], Denis Kress[1] and Aidar Kuttiubaev[4]

[1]Institute of Geotechnical Mechanics named by N. Poljakov of National Academy of Sciences of Ukraine, Simferopolska, 2a, Dnipro, 49005, Ukraine
[2]Ukrainian State University of Science and Technologies, Lazaryana Str., 2, Dnipro, 49010, Ukraine
[3]Ukrainian State University of Chemical Technology, Haharina Ave., 8, Dnipro, 49005, Ukraine
[4]Satbayev University, Satpaeva Str., 22, Almaty, 050000, Kazakhstan

[5]Corresponding author: vleonid1937@gmail.com

Abstract. Prof. L.I. Baron identified five forms of destruction during uniaxial compression of samples of regular geometry of rocks including truncated wedge, wedge, diagonal, longitudinal, and explosive forms. All of them are commonly characterized by the destruction of samples in their central parts showing two or more cracks, while the trajectories of crack development align with the corner points of the samples. Recently, was unexpectedly discovered a spall fracture in the form of a single crack emerged from the side wall of the specimen and propagating into it under uniaxial compression. Based on the discovery, the method for creating stress-strain diagrams for high rock samples was developed using four rock properties such as rock shear resistance limit, contact friction ratio, internal friction ratio, and modulus of elasticity. The stress-strain diagram of the spall fracture of high samples is described by a descending curve, which is typical for the diagrams of fracture created by two adjacent cracks of regular geometry samples. The maximum stresses required for the destruction of high rock samples are lower than those for the destruction of regular geometry samples of rocks with similar physical and mechanical properties.

1. Introduction

One of the important informative characteristics necessary to control the stress-strain state of rocks and their effective destruction on the disintegrating device. The important informative characteristics are the ultimate strength and residual strength of the samples, determined by the longitudinal stress-strain diagrams of their ultimate strength destruction [1-8].

In Ukraine, since the 1960s, these characteristics have been taken on special presses, which are available in certain research institutes, for example, in the Institute of Geotechnical Mechanics of the National Academy of Sciences of Ukraine and Kryvyi Rih National University. However, these works require highly qualified personnel, and the equipment is located far from the consumer, where up-to-date information about the properties of rocks is required. Therefore, there is a need to develop analytical methods for calculating the ultimate and residual strength of samples while knowing the properties of rocks determined by simple methods available to mining enterprises.

Previously, attempts were made to mathematically model the destruction of samples [9–15]. But these models have not been tailored to the level of complete analytical methods for calculating the parameters of the "normal stress–longitudinal strain" diagrams of the rock samples' ultimate fracture.

To determine the experimental ultimate strength of rocks, prismatic or cylindrical samples are used. Detailed methods for the analytical determination of the ultimate strength for prismatic samples are described in the book [16]. The authors used five experimental forms of destruction of regular geometry samples, established by prof. L.I. Baron [1, 2]: truncated wedge, wedge, diagonal, longitudinal, and explosive forms. The term "samples of regular geometry" refers to samples of only cubic or cylindrical geometry, in which $h/d = 1$ (where h - the height, m; d is the sample diameter, m). It should be noted that we are talking about the destruction of monolithic, non-layered samples, and not about the phenomenon of cleavage along the plane of oblique layering in the rock the sample was made of. All forms according to L. I. Baron are commonly characterized by the destruction of samples in their central part showing two or more cracks, while the trajectories of crack development align with the corner points of the samples. For many years, other forms of destruction were not encountered in the literature. Recently, we have unexpectedly discovered a spall fracture form under uniaxial compression of high samples, which is completely different from the forms according to L. I. Baron. It is a single crack emerging from the side wall of the sample and propagating into it, forming a piece $m_1\ d_1\ c_1$ (figure 1). In the figure, we have schematically depicted the formation of the trajectories of the maximum effective shear stresses (TMESS) under uniaxial compression of a high specimen on the sides of which cracks appear and develop.

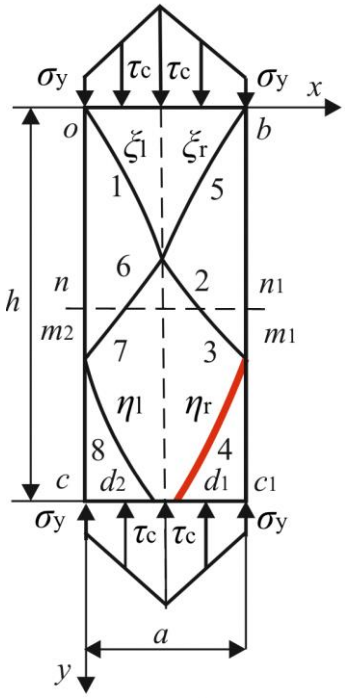

Figure 1. Scheme τ_c of a side crack formation in the sample: ox and oy axes; o, b, c, c_1 – sample corner points; n–n_1 – the horizontal axis of symmetry; a and h - the width (length) and height of the sample; σ_y – vertical normal stresses τ_c – contact tangential stresses; ξ_l, ξ_r, η_l and η_r – TMESS; m and m_1 – the exit points of TMESS ξ_l and ξ_r on the side surface; d_1 and d_2 – the exit points to TMESS n_l and n_r to the lower contact plane.

On the basis of the figure, we formulate the purpose of the article which is to develop a method for calculating the parameters of the "stress - strain" diagram of the high sample destruction.

2. Methods

As a destruction criterion, we take the Coulomb formula used in rock mechanics in τ_c

$$\tau_e = |\tau_\alpha| - \mu\sigma_\alpha \le k\ , \tag{1}$$

where τ_e – effective shear stress, Pa; τ_α – active shear stress, Pa; μ – internal friction ratio; σ_α – normal stress on the effective shear stress trajectory, Pa; k – rock shear resistance limit, Pa.

In formula (1) the parameter τ_e is represented as the external effective shear stress (EES) counteracted by the shear strength k inside the material. As long as the active shear stress, with the exception of internal friction losses, has not reached the maximum possible value of the internal shear resistance k for the given conditions, a stable balance of forces is maintained. When τ_e exceeds the value of k a crack is formed at some point.

Equation (1) in principal normal stresses is as follows

$$\tau_e = -\frac{\sigma_x - \sigma_y}{2}\sin 2\alpha + \tau_c\left(1-\frac{2y}{h}\right)\cos 2\alpha - \mu\left(\frac{\sigma_x + \sigma_y}{2} - \frac{\sigma_x - \sigma_y}{2}\cos 2\alpha - \tau_c\left(1-\frac{2y}{h}\right)\sin 2\alpha\right) \le k, \quad (2)$$

where σ_x and σ_y – horizontal and vertical normal stresses, Pa; τ_c – contact shear stress, Pa; α – the slope angle of TMESS, rad; y – ordinate of the considered point, m; h – the sample height, m.

We assume that the horizontal shear stresses (τ_c, Pa) according to the Amonton-Coulomb law are expressed by the formula

$$\tau_c = f_c\, \sigma_{y,} \quad (3)$$

where f_c – contact friction ratio.

Horizontal normal stresses during uniaxial compression of the sample arise from contact friction between the sample and the loading plate and are described by the formula [17, 18]

$$\sigma_x = \frac{2\left(k+\mu\sigma_y\right)}{\cos\rho}\left(\sin\rho - \sqrt{1-b^2}\right) + \sigma_y, \quad (4)$$

where

$$b = \frac{f_c\left(1-\frac{2y}{h}\right)\sigma_y}{\left(k+\mu\sigma_y\right)}. \quad (5)$$

The expression $f_c\left(1-\frac{2y}{h}\right)\sigma_y = \tau_{xy}$ indicates the attenuation of contact shear stresses along the longitudinal axis of the sample. The slope angle (α, rad) TMESS to attain the maximum value of τ_e is determined by the zero value of the derivative (2) in the above expression.

Then,

$$\mathrm{tg}2\alpha = -\frac{\left(\sigma_x - \sigma_y\right) - 2\mu\tau_{xy}}{\mu\left(\sigma_x - \sigma_y\right) + 2\tau_{xy}}, \quad (6)$$

where τ_{xy} – horizontal shear stress, Pa.

Each form of destruction of samples has its own characteristics. A common feature of the fracture forms described in the book [16], in contrast to the form shown in figure 1, is the exit of TMESS from the sample corners from above and below to the opposite contact surface. According to figure 1, the TMESS s come out on the side walls of the high sample. To determine the points m_1 and m_2 of the TMESS exit to the side walls, a program for a PC was developed according to the method from the book [16]. The distribution of contact normal stresses from above and below (figure 1) is described according to L. Prandtl's law by the formula

$$\sigma_{yi} = \sigma_{y0}\left(1 + \frac{2 f_c \cdot x}{h}\right), \quad (7)$$

and tangents is described by the formula

$$\tau_{xy} = \sigma_{y0}\left(1+\frac{2f_c\left(1-\frac{2y}{h}\right)\cdot x}{h}\right), \quad (8)$$

where σ_{yi} – current value of normal stresses, Pa; σ_{y0} – normal stress at the corner point, Pa; x – the abscissa of the point under consideration, m.

L. Prandtl [16] proved that the normal stresses remain constant along their action. In the mentioned book, we have proved that these formulas are also applicable inside the sample when σ_{y0} is replaced by σ_y which is the normal stress at the crack tip. Under contact loading, contact shear stresses develop inside bodies, as shown in figure 1. In the figure, vertical normal stresses applied from above and below the sample are shown in the form of triangles and described by formula (7). During longitudinal compression, friction forces that are directed against transverse deformation appear between the sample and the loading plates. These friction forces are represented by horizontal tangential stresses (τ_c, Pa), directed inside the sample and described by formula (8). The trajectories (TMESS) along which deformations develop, up to destructive ones, are indicated by ξ_l (left), ξ_r (right). η_l (left) and η_r (right) TMESS are shown schematically with rotations reflecting the effect of tangential stresses on them from contact friction.

The calculation is carried out in two stages. In the first stage, the exit point of TMESS on the side surface of the sample is determined. Note that the strength of the samples, in addition to the shear strength of the material, is also determined by the magnitude of the change in the TMESS angles due to contact friction.

The trajectories of maximum shear stresses are determined by the formula (6), and the normal stress (σ_{y_ξ}, Pa) at the crack tip is determined by the formula

$$\sigma_{y_\xi} = \frac{1}{\mu}\left(\frac{k\cdot\left(1+\sin\rho\sqrt{1-b_\xi^2}\right)\cdot\exp\left(2\mu\left(\beta_\xi+\beta_{m_1}\right)\right)}{1+\sin\rho\sqrt{1-b_\xi^2}}-k_{m_1}\right); \quad (9)$$

$$k_{m_1} = \frac{\left(k+\mu\sigma_{y_\xi}\right)\cdot\left(1+\sin\rho\sqrt{1-b_\xi^2}\right)}{\left(1+\sin\rho\sqrt{1-b_{m_1}^2}\right)\cdot\exp\left(4\mu\beta_{m_1}\right)}; \quad (10)$$

$$b_\xi = \frac{f_c\cdot\left(1-\frac{2y}{h}\right)\cdot\sigma_{y_\xi}\cdot\left(1+\frac{2f_c\cdot x_\xi}{h}\right)}{k\ +\mu\sigma_{y_\xi}\cdot\left(1+\frac{2f_c\cdot x_\xi}{h}\right)}; \quad (11)$$

$$b_{m_1} = \frac{f_c\cdot\sigma_{y_\xi}\cdot\left(1+\frac{2f_c\cdot x_{m_1}}{h}\right)}{k_{m_1}+\mu\sigma_{y_\xi}\cdot\left(1+\frac{2f_c\cdot x_{m_1}}{h}\right)}; \quad (12)$$

$$\beta_\xi = \frac{1}{2}\operatorname{arctg}\frac{b_\xi\cdot\cos\rho}{\sin\rho-\sqrt{1-b_\xi^2}}; \quad (13)$$

$$\beta_{m_1} = \frac{1}{2}\operatorname{arctg}\frac{b_{m_1}\cdot\cos\rho}{\sin\rho-\sqrt{1-b_{m_1}^2}}. \quad (14)$$

where k – the rock shear resistance limit, Pa; b_ξ – the ratio of horizontal shear stresses from contact friction to shear stresses from shear strength of the material and from internal friction at the crack tip; x_ξ – the abscissa of the crack tip, m; b_{m1}– the ratio of horizontal shear stresses from contact friction to shear stresses from shear strength of the material and from internal friction at the point where TMESS emerges on the side surface; x_{m1} – the abscissa of the TMESS exit point on the lateral surface. m; β_ξ – the angle of rotation TMESS due to contact friction at the crack tip, rad; β_{m1} – the angle of rotation TMESS from contact friction at the point of exit of TMESS to the side surface, rad; k_{m1} – shear stress on TMESS at the point of its exit to the side surface, Pa. By transforming the formula (6) we get the angle (rad) of TMESS inclination.

$$\alpha = \frac{\pi}{4}+\frac{\rho}{2}+\beta_\xi, \quad (15)$$

where ρ – the angle of internal friction, rad.

Let's write down the following initial conditions: k = 10 MPa; μ =1.0; ρ =45 rad; f_c=0.25; E = 500 MPa; h =2.5a; a = 1.

The book [16] shows that the formation of TMESS in one form or another aligns with the sample angles. For cubic samples, TMESS fits into the dimensions of the sample, enters one contact plane, and exits the opposite plane. Due to different rock strength values, commonly, there appears one crack that causes the development of another symmetrical crack. So, as in our case (figure 1), the left trajectory TMESS does not fit into the dimensions of the sample and extends onto its side surface at the point m1. At this point, the horizontal shear stresses arising from contact friction are less than those on the contact plane due to their attenuation. It forms a point with minimal resistance to destruction. A crack develops from this point in the lower right quarter of the image. To determine the coordinates of the mentioned point, the system of equations [6] and [9] - [17] was used with a slight correction of the sign from minus to plus in the formula (12), which was verified when creating stress-strain diagrams for the fracture forms of the samples considered in the book [16]. The calculation results in the point m_1 with coordinates x_0 = 1a and y_0=2a. Now it is necessary to determine a new TMESS, along which a crack will appear and develop.

But when choosing signs in expressions (11) and (12), the equality condition is k_{m1}= k exit TMESS at the point m_1 on the lateral surface. Then another TMESS η is formed and its slope angle is determined by the formula obtained from the expression (6) transformation:

$$\alpha_\eta = \frac{3\pi}{4}+\frac{\rho}{2}+\beta_{\eta_1}, \quad (16)$$

where α_η - trajectory inclination angle TMESS horizontal plane; $\beta_{\eta l}$ - trajectory rotation angle at the crack tip due to contact friction.

The signs in expressions (11) and (12) remain positive, and to match the equality k_{ml}= k at the point d_1 you need to use the minus sign in the exponents of formulas (9) and (10). Then, based on the solution of the systems (9) - (14) and formula (16), we will obtain the curve $m_l d_l$ (figure 1).

3. Results and discussion

Now, using the numerical values of the previously given four physical and mechanical properties of the rock, we can build a stress-strain diagram. The diagram is built on the following principle. Knowing the value of coordinates and stresses of τ_e of the tops of one or two cracks at each moment, we can determine the bearing part of the sample material, which is equal to the initial area of the latter minus the part of its area that was released from the load during the development of the crack. The part

of the sample released from the load is determined by using the values of the crack tip abscissa as $x = y \cdot \mathrm{ctg}\alpha$. Knowing the stresses σ_y at the crack tip, its coordinates, and the distribution function of contact stresses on the part that is still under the load (the bearing part of the sample), it is possible to determine the strength value of the sample if you have the values of three properties including the shear strength limit *k*, external and internal friction ratios, and if you know the fourth parameter *E* - the modulus of elasticity, MPa you can determine the parameters of the stress-strain diagram. A more detailed description of the formation of common forms of fracture is given in the book [16]. We use ready-made formulas borrowed from the mentioned book for one crack, and determine the parameters of the conditional stress-strain diagram

$$\sigma_c = \sigma_{y\xi}\left(\frac{\left(a - x_\xi\right)}{a} + \frac{f_c\left(a - x_\xi\right)^2}{2ha}\right), \tag{17}$$

$$\varepsilon = \frac{p}{E}, \tag{18}$$

$$p = \frac{\sigma_c}{a_1 - x_\xi}, \tag{19}$$

where σ_c – current strength value, Pa; x_ξ – crack tip abscissa, m; ε – longitudinal deformation; p – specific force, Pa; E –Young's modulus of elasticity.

Figure 2 shows the stress-strain diagram for k = 10 MPa, ρ = 45°, f_c = 0.25, E = 5000 MPa during the development of a crack $m_1 d_1$ (figure 1). The maximum stress was 138 MPa, which is significantly lower than the stress of 603 MPa required to fracture a rock sample of regular geometry with the same properties [16].

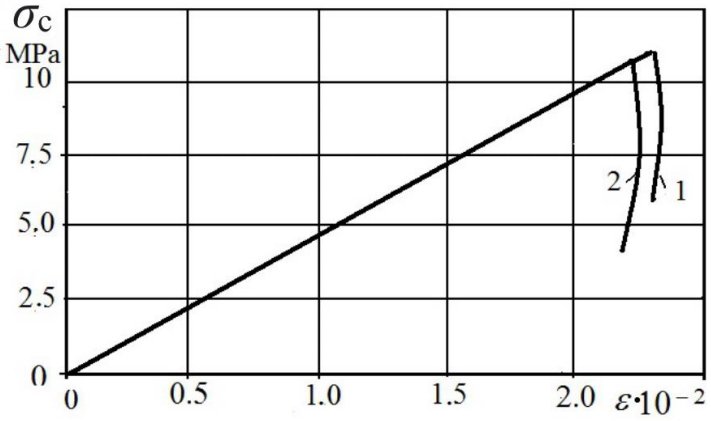

1 – *a*=1 m, *h*=2.5 m; 2 – *a*=1 m, *h*=3 m

Figure 2. Diagram "stress - longitudinal strain" at the destruction of a high sample.

It is also important to pay attention to the fact that for one spall crack, the diagram is described by a descending curve, in contrast to the fracture forms described by L. I. Baron. The authors of the book [16] found out that crushing rock samples of regular geometry featuring $\rho > 20°$, $f_c > 0.18$ causes the formation of two adjacent cracks. When a crack is formed in one of the corners of the sample, the diagram is described by an increasing stress curve that exceeds the stress limits in adjacent corners and causes the development of a second crack.

4. Conclusion

1. Prof. L.I. Baron identified five forms of fracture during uniaxial compression of rock samples of regular geometry and the trajectories of crack development, in which they align with their corner points. We have also discovered a spall fracture in the form of a single crack emerging from the lateral surface on high samples.

2. A method has been developed for creating stress-strain diagrams for high rock samples using four rock properties (k, f_c, μ, E).

3. The "stress-strain" diagram of the spall fracture of high samples is described by a descending curve, which is typical for the fracture diagrams of two adjacent cracks of samples of regular geometry with their truncated-wedge fracture.

4. The maximum stresses required for the destruction of high rock samples are lower than those for the destruction of rock samples of the regular geometry with the same properties.

References

[1] Petukhov I M 1978 *Osnovy Teorii Vnezapnykh Vybrosov Uglya, Porody i Gaza*. (Moskva: Nedra) pp 62-91
[2] Vinogradov V V 1989 *Geomekhanika Upravleniya Sostoyaniyem Massiva Vblizi Gornykh Vyrabotok* (Kyiv: Naukova dumka)
[3] Kirnichanskiy G T 1989 *Elementy Teorii Deformirovaniya i Razrusheniya Gornykh Porod* (Kyiv: Naukova dumka)
[4] Nesmashnyy Y A 2001 *Optimizatsiya Geometricheskiikh Parametrov Otkrygornykh Vyrabotok* (Krivoy Rog: Mineral)
[5] Nesmashnyy Y A and Bolotnikov A V 2017 *Metallurgicheskaya i Gornorudnaya Promyshlennost* (3) pp 82-87
[6] Bingxiang H and Jiangwei L 2013 *International Journal of Rock Mechanics and Mining Sciences* **61** pp 23-30
[7] James P. Meyer and Joseph F. Labuz 2013 *International Journal of Rock Mechanics and Mining Sciences* **60** pp 180-187
[8] Tarasov B and Potvin Y 2013 *International Journal of Rock Mechanics and Mining Sciences* **59** pp 57-69
[9] Chanyshev A I Abdulin I M 2008 *Kharakteristiki i Sootnosheniya na Kharakteristikakh na Zapredelnoy Stadii Deformirovaniya Gornykh Porod* (5) pp 27 – 41
[10] Lavrinov S V Revuzhenko A F 2017 *Modelirovaniye protsessov Deformirovaniya Samonapryazhennykh Obraztsov Gornykh porod*(1) pp 5 – 24
[11] Olovyannyy A G 2012 *Mekhanika Gornykh Porod. Modelirovaniye Razrusheniy*. (Saint Petersburg: "Izdatelsko-Poligraficheskaya Kompaniya "KOSTA")
[12] Kurguzov V D 2019 *Sravnitelnyy Analiz Kriteriyev Razrusheniya Isskusstvennykh Materialov i Gornykh Porod* (5) pp 79-89
[13] Kostandov Yu A 2016 *O Vliyanii kontaktnykh Usloviy na Otsenki Predelnykh Parametrov Moduley Uprugosti i Kharaktera Razrusheniya Szhimayemykh Obraztsov* (1) pp 82 -90
[14] Vasyliev L M, Vasyliev D L, Malich N G and Angelovskiy A A 2018 *Mekhanika Obrazovaniya Form Razrusheniya Obraztsov Gornykh Porod Pri ih Szhatii* (Dnipro: IMA-press)
[15] Vasyliev L M and Vasyliev D L 2013 *Teoreticheskoye Obosnovaniye Formirovaniya Gorizontalnykh Normalnykh Napryazheniy v Massivakh Gornykh Porod* (2) pp 81-90
[16] Vasyliev L M and Vasyliev D L 2013 *Journal of Mining Science* **49** pp 240-247
[17] Kozhevnykov A O, Dreus A Y, Liu B and Sudakov A K 2018 *Drilling fluid circulation rate influence on the contact temperature during borehole drilling* (Dnipro: Naukovyi Visnyk Natsionalnoho Hirnychoho Universytetu) pp. 35-42
[18] Bulat A, Blyuss B, Dreus A, Liu B and Dziuba S 2019 *Modelling of deep wells thermal modes* (Dnipro: Mining of Mineral Deposits) pp. 58-65